Identification of RRM2 as a key regulator of malignant epithelial cells in gastric cancer through single-cell transcriptomics

XINZHEN CAI[1*], YUN HE[2*], LILI KANG[1], DONGLI ZHOU[3], MENGMENG WANG[1] and TIANYU MA[3]

[1]Department of Rheumatology and Immunology, Gaoyou People's Hospital, Gaoyou, Jiangsu 225600, P.R. China; [2]Department of Oncology, Changshu Hospital Affiliated to Nanjing University of Chinese Medicine, Changshu, Jiangsu 215500, P.R. China; [3]Department of Oncology, Gaoyou People's Hospital, Gaoyou, Jiangsu 225600, P.R. China

Received August 26, 2025; Accepted February 17, 2026

DOI: 10.3892/or.2026.9159

Abstract. Gastric cancer (GC) is one of the most prevalent and life-threatening malignancies of the digestive tract worldwide. Ribonucleotide reductase regulatory subunit M2 (RRM2), a rate-limiting subunit in deoxyribonucleotide synthesis, is overexpressed and is associated with a poor prognosis in various solid tumors. However, its functional role and mechanisms in GC-specific malignant epithelial cell populations remain unclear. Single-cell transcriptomic data from GC and adjacent normal tissues were analyzed. Key malignant epithelial cell populations were identified using inferCNV, pseudotime trajectory analysis, and weighted gene co-expression network analysis. RRM2 was identified as a core gene by integrating data from TCGA-STAD, GSE66229, and GSE84433 datasets and analyzing its clinical relevance. To evaluate the biological effects of RRM2, functional assays, including colony formation, apoptosis, Transwell migration, and wound healing assays, were performed using AGS and HGC-27 GC cells with RRM2 knockdown. DNA damage was assessed using the alkaline comet assay and phosphorylated histone H2AX (γH2AX) immunofluorescence, and the expression of DNA damage repair-related proteins [including γH2AX, phosphorylated tumor protein p53 (p-p53), RAD51 recombinase (RAD51), poly(ADP-ribose) polymerase 1 (PARP-1), and X-ray repair cross-complementing protein 1 (XRCC1)] was examined using western blotting. Through analysis of gastric epithelial cell populations, a major malignant epithelial effector population in GC was identified, enriched in cells with active DNA replication and repair. Differentially expressed genes specific to this population were intersected with prognostic genes from GEO GC datasets, resulting in the identification of RRM2 as a key effector gene. Transcriptomic analysis revealed that high RRM2 expression was associated with an active immune microenvironment. Functional assays showed that RRM2 knockdown significantly inhibited GC cell proliferation and migration while promoting apoptosis. In addition, RRM2 knockdown exacerbated DNA damage, upregulated p-p53, and downregulated RAD51, with no significant effects on PARP-1 or XRCC1 expression. Collectively, RRM2 was shown to be a crucial regulator of the malignant phenotype of gastric epithelial cells. It promoted GC cell proliferation, invasion, and migration and modulated DNA damage and homologous recombination repair. In addition, RRM2 influenced the tumor immune microenvironment, highlighting its potential as a driver of malignant progression and a promising target for immunotherapy in GC.

Correspondence to: Dr Tianyu Ma, Department of Oncology, Gaoyou People's Hospital, 116 Fuqian Street, Gaoyou, Jiangsu 225600, P.R. China
E-mail: matianyu19820107@163.com

Dr Mengmeng Wang, Department of Rheumatology and Immunology, Gaoyou People's Hospital, 116 Fuqian Street, Gaoyou, Jiangsu 225600, P.R. China
E-mail: 407394034@qq.com

*Contributed equally

Abbreviations: GC, gastric cancer; dNTP, deoxynucleotide triphosphate; RRM2, ribonucleotide reductase regulatory subunit M2; WGCNA, weighted gene co-expression network analysis; DDR, DNA damage response; OS, overall survival; DSB, DNA double-strand breaks; HR, homologous recombination; BER, base excision repair; SSB, single-strand break; CNV, copy number variations; GSEA, gene set enrichment analysis; p-p53, phosphorylated tumor protein p53

Key words: GC, RRM2, DDR, DNA HR repair, single-cell RNA sequencing, epithelial cells

Introduction

Gastric cancer (GC), a malignant tumor originating from the gastric mucosal epithelium, occurs owing to a disruption in the dynamic balance between the proliferation and apoptosis of epithelial cells under the influence of various carcinogenic factors (1,2). GC is the fifth most common cancer worldwide and exhibits particularly high incidence rates of ~23.0 per 100,000 in males and ~9.7 per 100,000 in females in East Asian countries such as China, Japan, and South Korea (3,4). Despite advances in molecular targeted therapy and immunotherapy, the overall 5-year survival rate of patients with advanced GC remains <50% (5,6). Moreover, highly sensitive and specific biomarkers that can be used for early

screening, treatment monitoring, and personalized therapy in GC are lacking (7).

Numerous studies have shown that the initiation and progression of GC are closely associated with molecular alterations in key biological processes, such as the proliferation and apoptosis of malignant epithelial cells and epithelial-mesenchymal transition (EMT) (8-10). Therefore, elucidating the functional heterogeneity, molecular alterations, and the mechanisms driving these alterations in malignant gastric epithelial cells is necessary for identifying novel biomarkers and therapeutic targets with clinical translational potential, which is a key research focus in the field of precision medicine for GC.

During rapid proliferation, malignant gastric epithelial cells often exhibit increased genomic instability accompanied by extensive DNA damage (11). These cells typically activate DNA damage response (DDR) pathways to repair damaged DNA, preserve genomic integrity, and ensure continuous proliferation (12,13). In various DNA repair pathways, such as double-strand break (DSB) repair, base excision repair (BER), and homologous recombination (HR) repair, deoxyribonucleotide triphosphates (dNTPs) serve as the essential building blocks for DNA synthesis (14). Insufficient dNTP pools impair DNA repair, resulting in chromosome breakage and cell death (15). dNTP synthesis is tightly regulated by the rate-limiting enzyme ribonucleotide reductase (RNR), which contains a catalytic subunit, ribonucleotide reductase M1(RRM1), and a regulatory subunit, ribonucleotide reductase M2 (RRM2) (16).

Recent studies have identified RRM2 as a crucial regulator of tumor progression in multiple cancer types (17,18). In lung adenocarcinoma, RRM2 has been associated with enhanced tumor cell proliferation and invasion. In hepatocellular and breast cancers, RRM2 has been reported to contribute to DNA repair, metastasis, and treatment resistance. Through analysis of data from The Cancer Genome Atlas (TCGA) (https://portal.gdc.cancer.gov/) and the Genotype-Tissue Expression (GTEx) project (https://www.gtexportal.org/), it was revealed that RRM2 may play a potential oncogenic role in hepatocellular carcinoma (19). A total of 2,509 breast cancer samples were downloaded from the METABRIC database (https://www.cbioportal.org/study?id=brca_metabric). Among patients with luminal A and normal breast cancer, as well as those with stage 1 and 2 breast cancer, patients with high RRM2 expression exhibited poorer overall survival (OS) and distant metastasis-free survival (20). Additionally, in a study involving 200 patients with breast cancer from the histopathology laboratory at the Oncology Center of Mansoura University (Mansoura Egypt), it was found that among the estrogen receptor-positive group, RRM2 expression was associated with a shorter disease-free survival period (21). These findings highlight the diverse regulatory roles of RRM2 in various tumors. However, its specific role and mechanisms in GC remain unclear. In the present study, single-cell transcriptomic data, bulk RNA-sequencing data, and *in vitro* functional experiments were integrated to characterize RRM2 expression and investigate its functional role in GC progression. The findings provide theoretical insights and experimental evidence supporting the potential of RRM2 as a therapeutic target for GC.

Materials and methods

Gastric cancer cell culture. The GC cell lines AGS and HGC-27 were purchased from Procell Life Science & Technology Co., Ltd. Both cell lines were cultured in RMPI-1640 medium (cat. no. SH30809.01; HyClone; Cytiva) supplemented with 10% fetal bovine serum (cat. no. 10099141; Gibco; Thermo Fisher Scientific, Inc.) and 1% penicillin-streptomycin (cat. no. C0222; Beyotime Institute of Biotechnology) at 37˚C in an atmosphere containing 5% carbon dioxide. Mycoplasma contamination was assessed every 2 weeks using a Mycoplasma staining detection kit (cat. no. C0296; Beyotime Institute of Biotechnology).

Data sources and preprocessing. The gene expression data and clinical follow-up data of 370 patients with GC were obtained from TCGA database (TCGA-STAD dataset). The GSE66229 (22), GSE84433 (23) and GSE163558 (24) datasets were downloaded from the Gene Expression Omnibus (GEO) database. The data in these datasets were analyzed using the GPL570 HG-U133_Plus_2 Affymetrix Human Genome U133 Plus 2.0 Array (https://www.ncbi.nlm.nih.gov/geo/query/acc.cgi?acc=GPL570) and the GPL6947 Illumina HumanHT-12 V3.0 expression beadchip (https://www.ncbi.nlm.nih.gov/geo/query/acc.cgi?acc=GPL6947), respectively. The gene expression data and clinical follow-up data of 300 and 357 patients with GC were retained from the two datasets, respectively. Bioinformatics analyses were conducted using the following public databases: Tumor Immune Dysfunction and Exclusion (TIDE; http://tide.dfci.harvard.edu/) for predicting immune checkpoint inhibitor response; Tumor IMmune Estimation Resource (TIMER2.0; https://cistrome.shinyapps.io/timer/) for evaluating immune cell infiltration; TCGA (https://portal.gdc.cancer.gov/) for acquiring multi-omics GC data; GEO (https://www.ncbi.nlm.nih.gov/geo/) for validating differential gene expression; Kyoto Encyclopedia of Genes and Genomes (KEGG; https://www.kegg.jp/) for pathway enrichment analysis of differentially expressed genes; and Gene Ontology (GO; http://geneontology.org/) for functional annotation of gene sets.

Data analysis. Single-cell and transcriptome-wide sequencing were performed using the R software (version 4.5.1; https://www.r-project.org/). For single-cell RNA sequencing (scRNA seq), cell-level QC thresholds were applied as follows: cells with nCount-RNA between 1,000 and 60,000 and those with 500-7,000 genes (nFeature-RNA) were retained, whereas cells with a mitochondrial gene percentage of >20% were excluded. For gene-level QC thresholds, genes expressed in ≥5 cells were retained, and batch effects were corrected using the Harmony package (version 1.2.3; https://cran.r-project.org/web/packages/harmony/). Batch effects in expression data were corrected through quantile normalization using the normalizeBetweenArrays function in the limma package (version 3.46.0; https://bioconductor.org/packages/release/bioc/html/limma.html). Data reliability was validated through principal component analysis (PCA) implemented using the FactoMineR package (version 2.12; https://cran.r-project.org/web/packages/FactoMineR/), and PCA plots were generated using the ggplot2 package (version 3.5.2;

https://cran.r-project.org/web/packages/ggplot2/). Differential expression analysis was performed using the limma or DESeq2 package (version 1.49.4; https://bioconductor.org/packages/release/bioc/html/DESeq2.html); prognostic analysis was performed using the survival (version 3.8-3; https://cran.r-project.org/web/packages/survival/) and survminer (version 0.5.0; https://cran.r-project.org/web/packages/survminer/) packages; weighted gene co-expression network analysis (WGCNA) was performed using the WGCNA package (version 1.73; https://cran.r-project.org/web/packages/WGCNA/); cell-cell communication was analyzed using CellChat (version 2.1.2; https://github.com/jinworks/CellChat); pseudotime series analysis was performed using Monocle2 (version 2.36.0; bioconductor.org); and copy number variations (CNVs) were analyzed using the inferCNV package (version 1.24.0; https://bioconductor.org/packages/release/bioc/html/infercnv.html). Data were visualized using the ggplot2, ComplexHeatmap (version 2.25.2; bioconductor.org), and Seurat packages (version 5.3.1; cran.r-project.org). A flowchart demonstrating the detailed data processing protocol is shown in Fig. 1. scRNA QC parameters included nCount-RNA, nFeature-RNA, mitochondrial gene percentage and the number of genes expressed per cell.

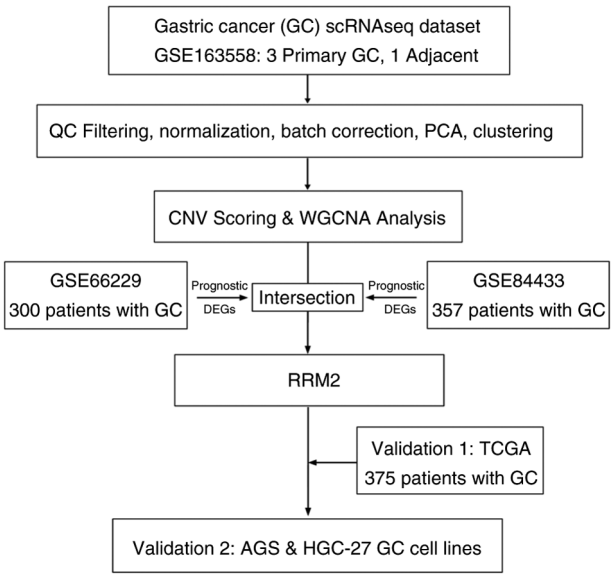

Figure 1. Flowchart of the analysis of the present study. GC, gastric cancer; scRNAseq, single-cell RNA sequencing; QC, quality control; PCA, principal component analysis; CNV, copy number variation; WGCNA, Weighted Gene Co-expression Network Analysis; DEGs, differentially expressed genes; RRM2, ribonucleotide reductase regulatory subunit M2; TCGA, The Cancer Genome Atlas.

siRNA cell transfection. AGS and HGC-27 cells in the logarithmic growth phase were seeded in 24-well plates and transfected when the cell density reached 80%. A total of 1.25 μl of 20 μM RRM2 siRNA (a negative control siRNA was included in the same kit; cat. no. HY-RS12286; MedChemExpress) was diluted with serum-free medium to a final volume of 50 μl, gently mixed, and incubated at room temperature for 5 min (solution A). Subsequently, 2.5 μl of siRNA/miRNA transfection reagent (cat. no. HY-K2017; MedChemExpress) was diluted with serum-free medium to a final volume of 50 μl, mixed gently and incubated at room temperature for 5 min (solution B). Solution B was gradually added dropwise to solution A, mixed gently and incubated at room temperature for 20 min to form a transfection complex (this mixture was used within 60 min). After the cell culture medium was removed, 400 μl of serum-free medium and 100 μl of the transfection complex were sequentially added and gently mixed. After 6 h, the medium was replaced with a complete medium containing serum, and incubation was continued. Protein extraction and western blotting were performed to assess RRM2 knockdown efficiency.

Colony formation assay. Cells in the logarithmic growth phase were seeded in a 6-well plate at a density of 500-1,000 cells/well, mixed evenly, and cultured for 14 days at 37˚C. After colonies were visible, the medium was removed, and the plates were washed twice with phosphate-buffered saline (PBS). Thereafter, the cells were fixed with 4% paraformaldehyde (cat. no. P0099-3L; Beyotime Insitute of Biotechnology) for 20 min at room temperature and stained with 0.1% crystal violet (cat. no. Y268091; Beyotime Insitute of Biotechnology) for 20 min at room temperature. After rinsing and air-drying, the cells were imaged and counted using the ImageJ software (version 2.14.0; National Institutes of Health).

Cell apoptosis assay. Cells ($3x10^5$) in the logarithmic growth phase were harvested, and the culture supernatant and digested cells were centrifuged separately at 300 x g for 5 min at 4˚C. The supernatants were discarded, and the pellets were combined, resuspended in binding buffer, and incubated with Annexin V-FITC and PI (cat. no. C1062M; Beyotime Insitute of Biotechnology) at 4˚C for 15 min in the dark. Flow cytometry (BD FACSVerse; BD Biosciences) was used to calculate the proportion of early apoptotic cells in the lower right quadrant (Annexin V-FITC$^+$ and PI$^-$), and the data were analyzed with FlowJo 10.4 (BD Biosciences).

Transwell assay. Transwell inserts (cat. no. 3422; Corning, Inc.) were purchased in advance. Logarithmically growing cells were digested and resuspended in serum-free medium. A total of 2,000 cells were counted and seeded into the upper chamber. The lower chamber was filled with complete medium containing 10% FBS. After 24 h of culture at 37˚C, the inserts were removed, washed twice with FBS, fixed with 4% paraformaldehyde for 20 min at room temperature and stained with crystal violet for 20 min at room temperature. Non-migrated cells were removed with a cotton swab, allowed to dry, and images were captured under a fluorescence microscope (Olympus IX73; Olympus Corporation). Cell counting and analysis were performed using ImageJ (version 2.14.0) software.

Wound healing assay. Logarithmically growing cells were seeded in a 6-well plate. When the cell confluence reached above 95%, a straight scratch was made in the cell layer using a sterile pipette tip. The scratched surface was gently rinsed with PBS. After imaging, 4% FBS-reduced serum medium was added and cultured for another 24 h (25). The supernatant was discarded, the cells were gently rinsed with PBS and images were obtained again. All images were captured under a fluorescence microscope (Olympus IX73; Olympus Corporation).

The width of the scratch was measured and analyzed using ImageJ software (version 2.14.0).

Alkaline comet electrophoresis. Using the Comet Electrophoresis Kit (cat. no. C2041S; Beyotime Institute of Biotechnology), approximately $1x10^4$ to $5x10^4$ cells in the logarithmic growth phase were mixed with 0.7% low-melting-point agarose and dropped onto pretreated slides. The mixture was incubated at 4˚C for 10 min. After the agarose solidified, the slides were placed in lysis buffer at 4˚C in the dark for at least 1 h. The slides were then denatured in alkaline electrophoresis buffer (300 mM NaOH, 1 mM EDTA, pH 13) for 60 min. Subsequently, electrophoresis was performed at 25 V for 30 min in the dark at 4˚C. Following electrophoresis, the cells were neutralized, stained with PI at 2 μg/ml for 10 min in the dark at room temperature, and observed under a fluorescence microscope (Olympus IX73; Olympus Corporation) and images were obtained.

Immunofluorescence. Using an immunofluorescence kit (cat. no. C2037S; Beyotime Institute of Biotechnology), cells in the logarithmically growing phase were seeded onto slides, removed from the slides, gently rinsed twice with PBS, fixed with 4% paraformaldehyde for 15 min at room temperature, permeabilized with 0.1% Triton X-100 (cat. no. NG1031A; Beyotime Insitute of Biotechnology) for 10 min, blocked with 5% BSA (cat. no. A8806; Sigma-Aldrich; Merck KGaA) for 1 h at 37˚C and incubated overnight at 4˚C with a dropwise diluted (1:500) primary antibody (γH2AX; cat. no. 9718S; Cell Signaling Technology, Inc.). The cells were rinsed twice with PBS, and diluted (1:100) fluorescently labeled (Alexa Fluor 488) donkey anti-rabbit IgG secondary antibodies (cat. no. ab150061; Abcam) were added for 1 h at room temperature. Cell nuclei were counterstained with DAPI for 10 min at room temperature, then mounted and observed and photographed under a fluorescence microscope.

Western blot analyses. Cells in the logarithmically growing phase were centrifuged at 300 x g for 5 min at room temperature, the supernatant discarded, and the pellet added to lysis buffer (cat. no. P0013B; Beyotime Insitute of Biotechnology). Total cellular protein was extracted and quantified using the BCA assay (cat. no. P0010; Beyotime Biotechnology). A total of 20 μg extracted proteins were subjected to 10% SDS-PAGE electrophoresis (60 V for 30 min and then transferred to 120 V for 60 min). After cutting the gel, the membrane was transferred to a PVDF membrane (300 mA for 100 min) and blocked with 5% skim milk for 2 h at room temperature. The membrane was then incubated with the primary antibody at 4˚C overnight, washed three times with TBST (including 0.1% Tween-20), and incubated with the diluted (1:1,000) secondary antibody (anti-rabbit IgG, HRP-linked antibody; cat. no. 7074; and anti-mouse IgG, HRP-linked antibody; cat. no. 7076; both from Cell Signaling Technology, Inc.) at room temperature for 2 h. After washing the membrane three times with TBST, the membrane was developed and photographed using ECL luminescent solution (NCM Biotech; Suzhou Xinsaimei Biotechnology Co., Ltd.), and the grayscale value of the bands was analyzed using ImageJ software (version 2.14.0). The primary antibodies used were as follows: Poly(ADP-ribose) polymerase 1 (PARP-1; cat. no. 9532T; Cell Signaling Technology, Inc.; diluted 1:1,000), X-ray repair cross-complementing protein 1 (XRCC1; cat. no. ET1704-01; Huabio; diluted 1:1,000), phosphorylated tumor protein p53 (p-p53; cat. no. HA722761; Huabio; diluted 1:2,000), RRM2 (cat. no. ET1705-62; Huabio; diluted 1:1,000), RAD51 recombinase (RAD51; cat. no. ET1705-96; Huabio; diluted 1:5,000), phosphorylated histone H2AX (γH2AX; cat. no. 9718S; Cell Signaling Technology, Inc.; diluted 1:1,000), GAPDH (cat. no. 2118S; Cell Signaling Technology, Inc.; diluted 1:1,000).

Statistical analysis. Each experiment was performed in triplicate or more. Data are presented as the mean ± standard deviation (SD). Statistical analyses and figure creation were conducted using GraphPad Prism 10 (Dotmatics). Comparisons between two groups (Figs. 5 and 6) were conducted using Student's t-test. One-way ANOVA was used for comparisons among mutliple groups (Fig. 4C and H). When a significant main effect ($P<0.05$) was found, pairwise comparisons between groups were further assessed using Tukey's post-hoc test. A $P<0.05$ was considered to indicate a statistically significant difference. The following significance levels were applied: $P<0.05$, $P<0.01$, $P<0.001$.

Results

Single-cell analysis indicates the key role of epithelial cells in GC progression. The scRNA-seq data of patients with GC were subjected to quality-control analysis and highly variable genes were selected (Fig. S1A-C). Cell populations were compared between tumor and normal tissues, and each cell cluster was annotated (Fig. 2A-C). The inferCNV algorithm was used to analyze CNVs across different cell populations. The results revealed that D-epithelial cells and general epithelial cell clusters exhibited a significantly high number of CNVs (Fig. 2D and E).

These two epithelial cell populations were subdivided into six clusters for further analysis. Among them, clusters 0 (C0) and 1 (C1) accounted for the largest proportions and were present only in tumor tissues (Fig. 2F and G). C0 (including genes such as KRT19, GABRP, GPRC5A, TMC5, CYP3A5, CD55, MYH14, S100P, KRT8 and ANXA2) exhibited an epithelial cell subtype with secretory/metabolic function in tumors. C1 (including genes such as TOP2A, MKI67, BIRC5, PBK, RRM2, CDC20, ASPM, CEP55, TPX2 and KIF20B) contained highly proliferating epithelial cells. To identify potential clinical molecular targets, analysis focused on the more abundant tumor epithelial cell subpopulation. Pseudotime trajectory analysis revealed that C1 cells were more primitive than C0 cells (Fig. 2H). Gene set enrichment analysis (GSEA) indicated that C1 cells were primarily enriched in DNA repair and MYC target-related pathways (Fig. 2I). Intercellular communication analysis revealed that both C0 and C1 cells strongly interacted with other epithelial cell populations (Fig. 2J). Except for C0 and C1, C2 represents a differentiated cell group with some characteristics of stem/progenitor cells from epithelial origin (including genes such as PGC, ALDH1A1, FAM3B, CXCL17, OLFM4, MT1M, REG1A, TCEAL9, CDKN2A and EID1). The C3

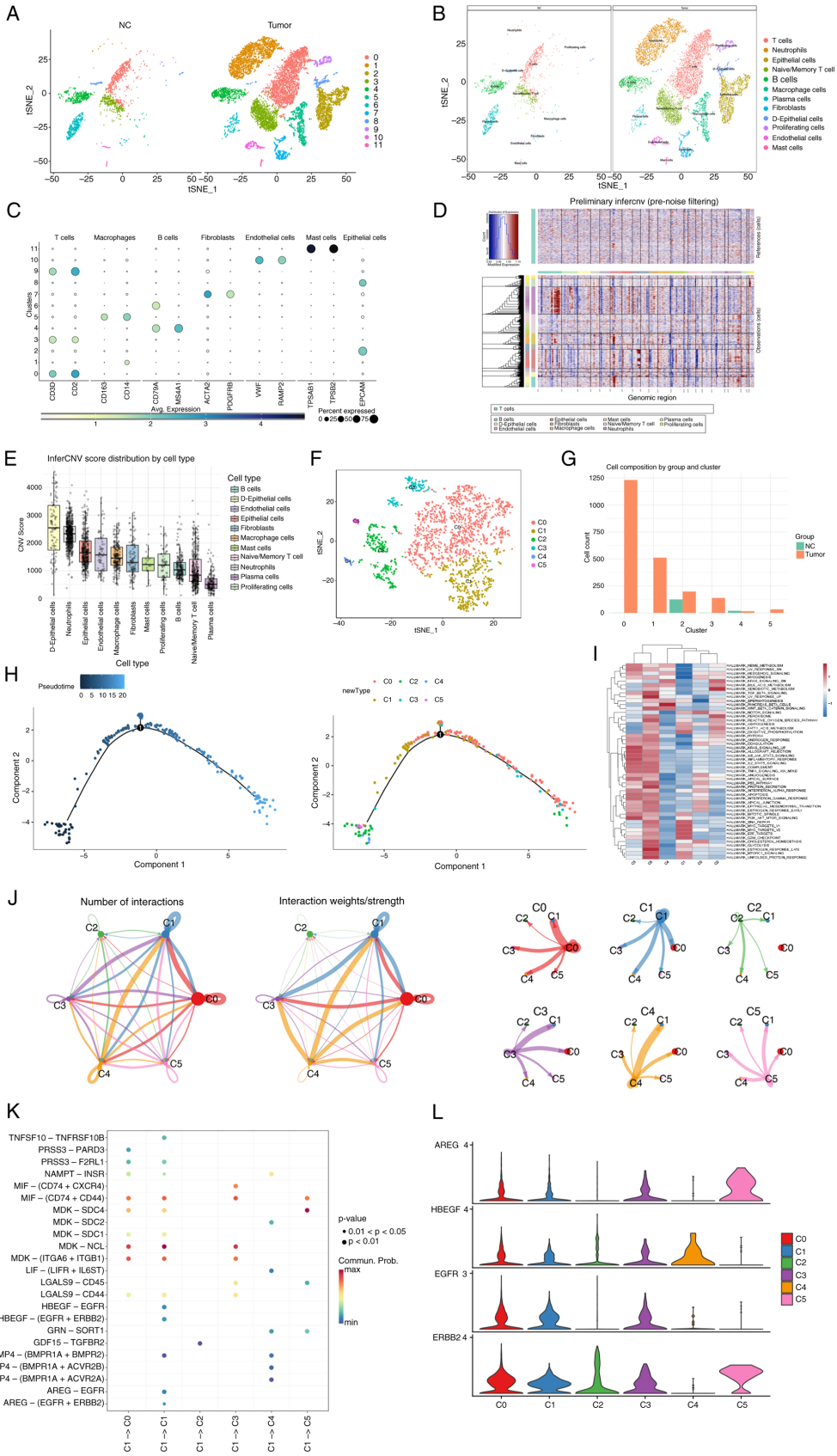

Figure 2. Single-cell analysis reveals the crucial role of epithelial cells in GC progression. (A and B) The single-cell dataset (GSE163558) was divided into normal and tumor groups and each cell cluster was annotated. (C) Expression patterns of marker genes in each cluster. (D) CNVs in each cell cluster were analyzed using the inferCNV algorithm. (E) D-epithelial cells and epithelial cell clusters exhibited a high frequency of CNVs. (F and G) Classification of D-epithelial and epithelial cells into six subgroups and their distributions in tumor and normal tissues. (H) Pseudotime trajectory analysis showing the developmental progression of each subgroup. (I) GSEA results showing gene functions enriched in the six subgroups. (J) Cell-cell communication analysis results showing interaction networks among the six subgroups. (K) Ligand-receptor interactions between cluster 1 and other clusters. (L) Expression patterns of the EGFR signaling pathway across the six subgroups. GC, gastric cancer; CNV, copy number variation; GSEA, gene set enrichment analysis; EGFR, epidermal growth factor receptor.

group corresponds to activated/effector T cells associated with epithelial cells (including genes such as CD2, FYB1, PTPRC, SAMSN1, WIPF1, SRGN, LCP1, CD52, LSP1 and SLA), while C4 comprises neuroendocrine-like epithelial cells (including genes such as RIMBP2, ST18, SCG5, HEPACAM2, SCG3, INSM1, RFX6, ARX, FGF14 and PCSK1). Finally, the C5 group represents an inflammatory/stress-responsive epithelial subpopulation (including genes such as NPPB, TNF, CYP2E1, CXCL5, HLA-DQA2, LY6K, CDKN2A, MYL9, TAGLN, PNMA5) (Table SI).

As shown in Fig. 2K, C1 cells were involved in extensive ligand-receptor interactions with other clusters. In addition, pathway enrichment analysis revealed activated EGFR, WNT, and BMP signaling in C1 (Figs. 2L and S1D).

Definition and identification of major effector cell subpopulations within epithelial cell clusters. GO and KEGG analyses revealed that C1 cells were predominantly enriched in the 'chromosomal region', 'ribonucleoprotein complex biogenesis', and 'ATP hydrolysis activity' and were closely associated with the 'cell cycle' and 'DNA replication'-related processes (Fig. 3A and B). Furthermore, WGCNA was performed on C1 cells, selecting a soft-threshold power of 8, and divided C1 into 28 subgroups (Fig. 3C and D). The associations among these subgroups are presented in Fig. 3E and F. Among the 28 modules identified by WGCNA, their associatons with the C0-C5 cell subpopulations (Fig. 3E) were systematically evaluated. In the association study between module 28 and subpopulation C1, four subclusters (C11, C127, C112, and C114) exhibited significantly higher average expression levels compared with other subclusters. Based on this observation, these four subclusters were selected for subsequent functional validation experiments (Fig. 3G). The key genes expressed in these subpopulations are shown in Fig. 3H.

Identification of RRM2 as a key molecular target through integrated transcriptomic analysis. GC-specific transcriptomic datasets GSE66229 and GSE84433 were obtained from GEO, and batch effects were removed. Differentially expressed genes (DEGs) associated with GC prognosis were identified based on survival analysis (Fig. S2A-D). Core genes from the four key malignant epithelial cell subclusters (C11, C112, C114, and C127) were intersected with the DEGs, resulting in the identification of two overlapping genes, RRM2 and PRNP. GO and KEGG enrichment analyses showed that RRM2 was strongly associated with 'DNA replication'; therefore, it was selected as the primary candidate molecular target for GC. Pan-cancer analysis revealed that RRM2 expression was significantly higher in tumor tissues than in adjacent normal tissues in various cancer types (Fig. 4A). In both GSE66229 and GSE84433 datasets, patients with GC were stratified into high- and low-RRM2-expression groups. Expression trend analysis showed that RRM2 expression gradually decreased with disease progression (Fig. 4B, C, G and H).

RRM2 expression was positively associated with the abundances of activated memory $CD4^+$ T cells, M0 and M1 macrophages, and resting NK cells (Fig. 4D and I). Using the TIMER database, it was found that high RRM2 expression in GC was associated with increased infiltration of $CD8^+$ T cells, $CD8^+$ naive T cells, cytotoxic lymphocytes (CTLs) and cytotoxic cells (Fig. S1E). The TIDE scores between two GEO GC datasets (GSE66229 and GSE84433) were compared. A high TIDE score indicates an increased risk of immune evasion by the tumor and is assoicated with a poorer prognosis for patients. Both datasets showed that the TIDE scores in the high-RRM2-expression group were lower than those in the low-RRM2-expression group, with statistically significant differences observed in GSE84433 dataset. These findings suggest that patients with GC with higher RRM2 expression may exhibit reduced immune evasion and potentially an improved response to immune checkpoint blockade therapy (Fig. S2E). The associations between RRM2 expression and prognosis across three datasets (GSE66229, GSE84433 and TCGA) are shown in Fig. 4E, J, and O. Notably, statistically significant differences are shown in Fig. 4E and O. In Fig. 4J, although P=0.088, a consistent trend is observed in which higher RRM2 expression is associated with longer survival time. It is hypothesized that if the GSE84433 dataset in Fig. 4J were expanded with additional data, it would likely achieve a $P<0.05$. KEGG analysis showed that RRM2 was enriched in 'DNA replication' and 'cell cycle' pathways (Fig. 4F and K). To validate these findings, patients with GC in the TCGA-STAD dataset were divided into RRM2-high (G1) and RRM2-low (G2) groups (Fig. 4L). G1 exhibited higher abundances of activated memory $CD4^+$ T cells, M0 and M1 macrophages and resting NK cells, as well as significantly higher expression levels of immune checkpoint genes such as LAG3, PDCD1, and CTLA4 (Fig. 4M and N). The results of GO and KEGG enrichment analyses in the TCGA-STAD dataset were consistent with those observed in the GSE66229 and GSE84433 datasets (Fig. S2G-I).

Functional validation of RRM2 in GC cells. To assess the role of RRM2 in GC progression, it was knocked down in two GC cell lines, AGS and HGC-27. Colony formation assay showed that RRM2 knockdown significantly suppressed colony formation in both cell lines (Fig. 5A and C), suggesting that RRM2 contributes to GC cell proliferation. In addition, RRM2 knockdown led to an increase in the number of apoptotic cells (Fig. 5B and C).

Transwell and wound healing assays showed that RRM2 knockdown reduced the number of GC cells migrating through the Transwell membrane and impaired the wound closure ability of the cells. These results suggest that RRM2 regulates the migratory abilities of GC cells (Fig. 5D-F).

RRM2 induces DNA damage and impairs DNA repair capacity in GC cells. Analysis of GC datasets from the GEO and TCGA databases indicated a strong association between RRM2 expression and DNA replication in GC. To validate this association, a comet assay was performed using GC cells transfected with control siRNA (CTRL group) or RRM2-targeting siRNA (siRRM2 group). The siRRM2 group exhibited pronounced comet tails and an increased tail DNA content, suggesting a significantly high proportion of DNA strand breaks (Fig. 6A). Consistently, γH2AX expression was markedly higher in the siRRM2 group than in the CTRL group, indicating substantial DNA damage upon RRM2 knockdown (Fig. 6B).

To examine the underlying mechanisms, the expression levels of proteins associated with DNA damage and repair were

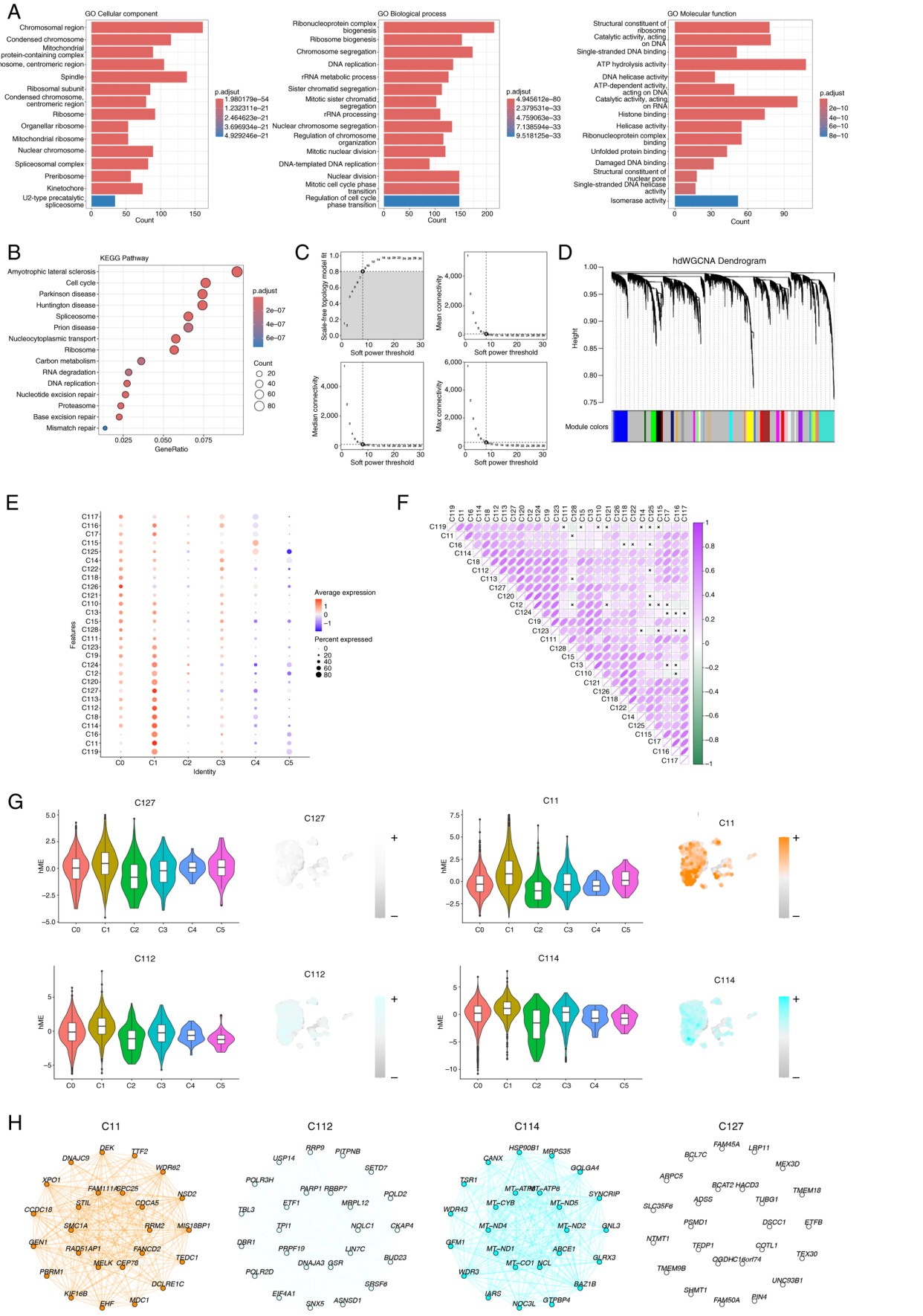

Figure 3. Identification and characterization of key effector cell populations within epithelial cell clusters. (A and B) GO and KEGG enrichment analyses of C1 to annotate its biological functions. (C) Selection of soft-threshold power for WGCNA. (D) Cluster dendrogram generated through WGCNA. (E) Expression patterns of WGCNA-derived gene modules in clusters 0-5 (C0-C5). (F) Association heatmap of WGCNA-derived gene modules. (G) Identification of C11, C127, C112, and C114 as the subclusters most closely associated with C1 and exhibiting the highest gene expression levels. (H) Hub genes in C11, C112, C114, and C127. GO, Gene Ontology; KEGG, Kyoto Encyclopedia of Genes and Genomes; WGCNA, Weighted Gene Co-expression Network Analysis.

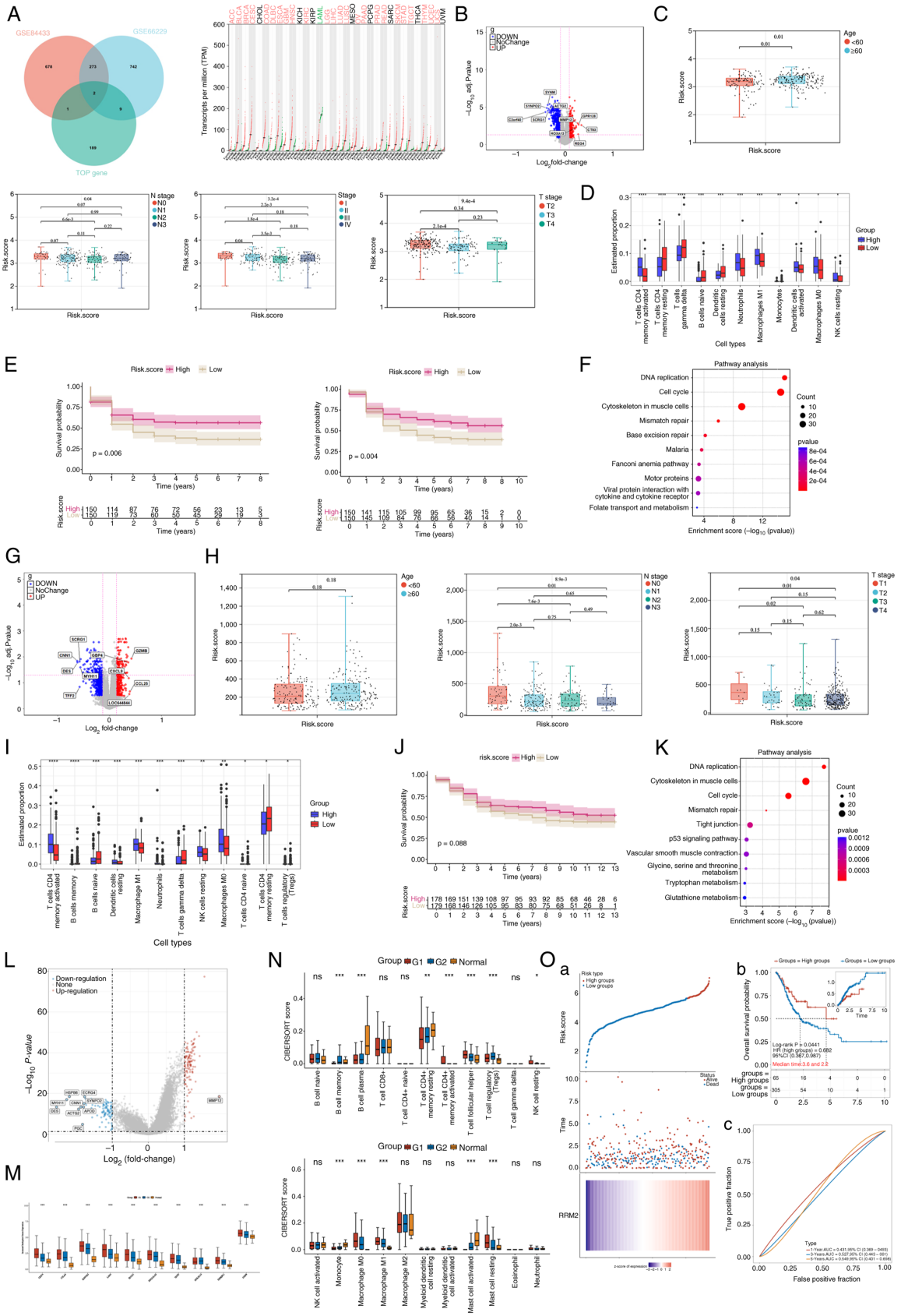

Figure 4. Identification of RRM2 as a key molecular target in GC based on transcriptomic data. (A) RRM2 was identified as a hub gene by intersecting prognosis-related DEGs from the GSE66229 and GSE84433 datasets with WGCNA-derived module genes. Its expression in tumor versus adjacent normal tissues across pan-cancer datasets is shown. (B, G and L) DEGs between the high- and low-RRM2-expression groups in the GSE66229, GSE84433, and TCGA-STAD datasets. (C and H) Association of RRM2 expression with age and TNM stage. (D, I and N) Association between RRM2 expression and immune cell infiltration. (E, J and O) Kaplan-Meier survival analyses indicating the prognostic significance of RRM2 in GC. (F and K) KEGG enrichment analysis showing RRM2-related pathways in GC. (M) Association between the expression of RRM2 and immune checkpoint genes. RRM2, ribonucleotide reductase regulatory subunit M2; GC, gastric cancer; DEGs, differentially expressed genes; WGCNA, Weighted Gene Co-expression Network Analysis; TCGA, The Cancer Genome Atlas; STAD, stomach adenocarcinoma; KEGG, Kyoto Encyclopedia of Genes and Genomes. *P<0.05, **P<0.01, ***P<0.001, ****P<0.0001.

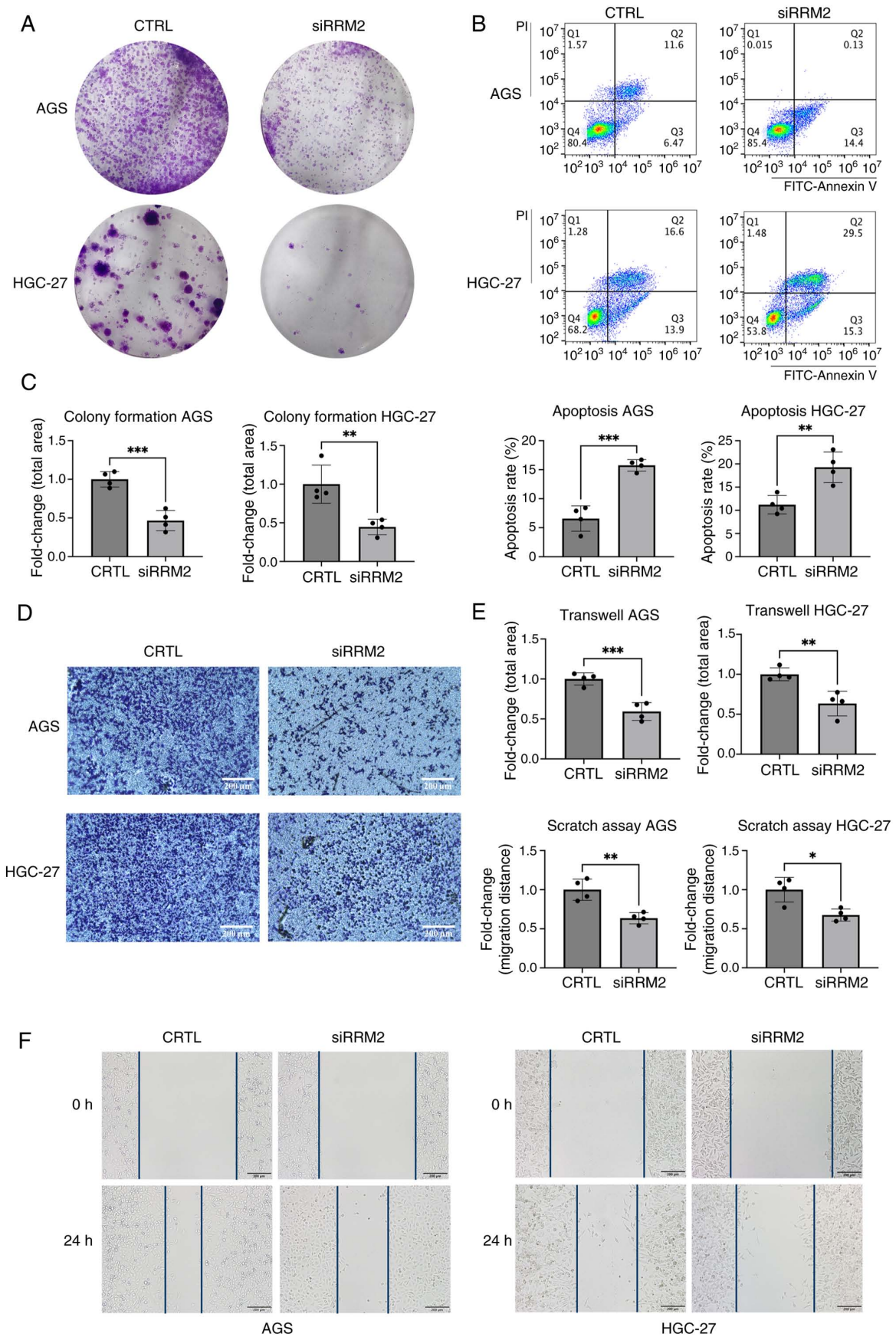

Figure 5. Functional validation of RRM2 in GC cells. (A) Colony formation assay of the two GC cell lines in the control and siRRM2 groups. (B) Apoptosis analysis of the two GC cell lines in the control and siRRM2 groups. (C) Quantification of the colony formation and apoptosis assay results. (D) Transwell migration assays of the two GC cell lines in the control and siRRM2 groups. Scale bar, 200 μm. (E) Quantification of the Transwell and wound healing assay results. (F) Wound healing assay of the two GC cell lines in the control and siRRM2 groups. In these experiments, each condition consisted of n=4 biological replicates, with each replicate analyzed in technical triplicate. RRM2, ribonucleotide reductase regulatory subunit M2; GC, gastric cancer; siRRM2, RRM2-targeting siRNA. *P<0.05, **P<0.01, ***P<0.001.

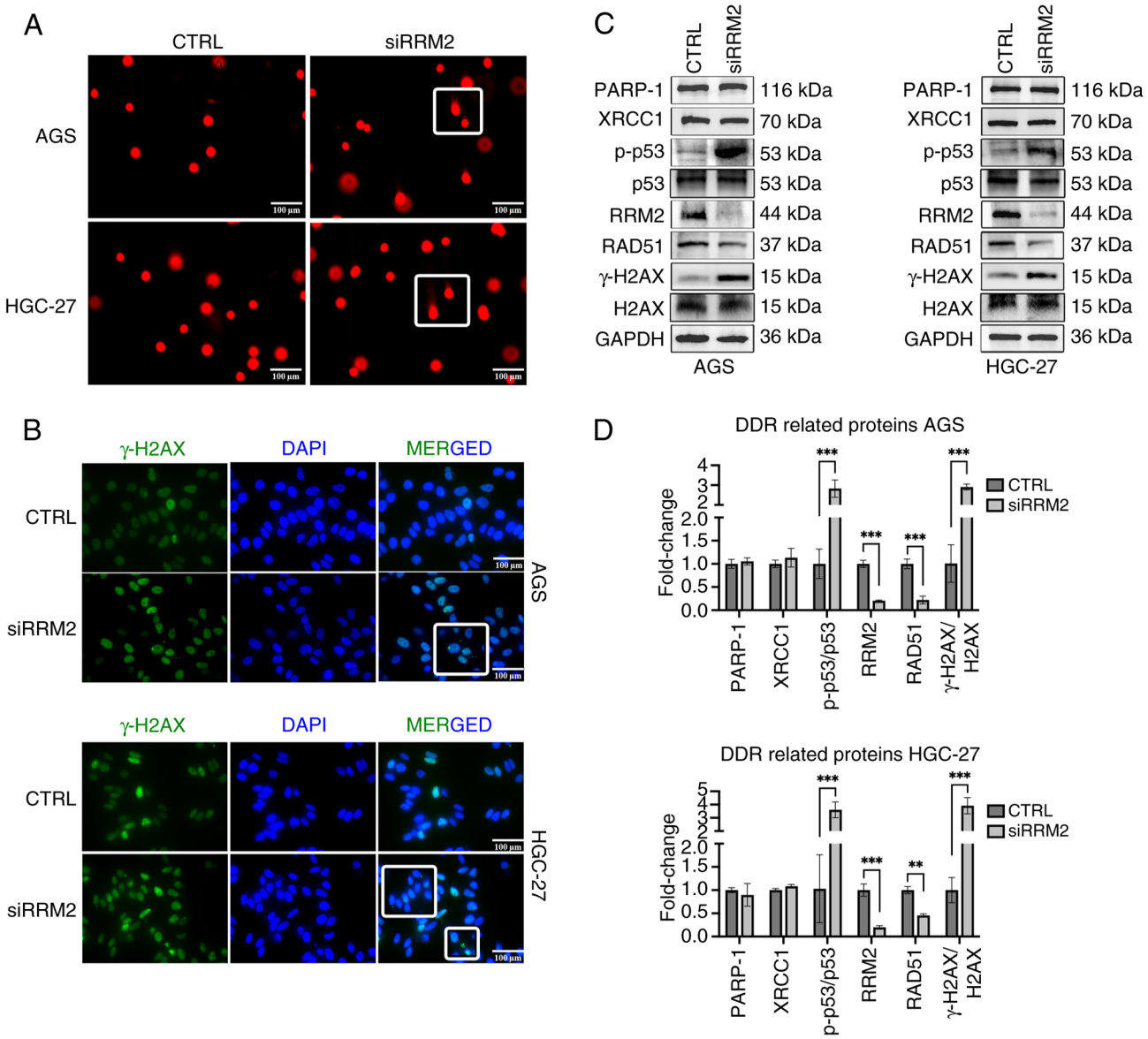

Figure 6. RRM2 induces DNA damage and impairs DNA repair capacity in GC cells. (A) Compared with the CTRL group, the siRRM2 group showed pronounced comet tails and an increased tail DNA content. Scale bar, 100 μm. (B) RRM2 knockdown markedly increased γH2AX expression in GC cells. Scale bar, 100 μm. (C and D) Compared with the CTRL group, the siRRM2 group showed significantly higher expression levels of γH2AX and p-p53 and lower expression levels of RAD51. No significant changes were observed in PARP-1 and XRCC1 expression. In these experiments, each condition consisted of n=3 biological replicates, with each replicate analyzed in technical triplicate. RRM2, ribonucleotide reductase regulatory subunit M2; GC, gastric cancer; CTRL, control; siRRM2, RRM2-targeting siRNA; γH2AX, phosphorylated histone H2AX; p-p53, phosphorylated tumor protein p53; RAD51, RAD51 recombinase; PARP-1, poly(ADP-ribose) polymerase 1; XRCC1, X-ray repair cross-complementing protein 1. **P<0.01, ***P<0.001.

assessed. Western blotting revealed that RRM2 knockdown increased the protein expression levels of the DDR markers γH2AX and p-p53 but significantly downregulated the HR repair marker RAD51. Conversely, the expression levels of PARP-1, a key protein in single-strand break (SSB) repair, and XRCC1, a key protein in BER, remained unchanged. These findings suggest that RRM2 depletion induces DNA damage and is associated with HR repair in GC cells (Fig. 6C and D).

Discussion

Recent studies have shown that RRM2 is highly expressed in various solid tumors and is closely associated with a poor prognosis and chemoresistance (26,27). Through scRNA-seq analysis of GC datasets, a subset of malignant epithelial cells specifically enriched within GC tissues were identified. Further analysis revealed that RRM2 played a functional role in the dominant effector cell subpopulations of malignant epithelial cells in GC. Numerous studies have confirmed that RRM2 acts as an oncogene in various cancers. In lung adenocarcinoma, RRM2 was shown to be associated with enhanced tumor cell proliferation and invasion (28). In head and neck cancers, RRM2 was revealed to contribute to apoptosis resistance by regulating Bcl-2. RRM2 promoted EMT in nasopharyngeal carcinoma by suppressing E-cadherin (29). In addition, RRM2 overexpression has been been shown to be associated with therapeutic resistance in pancreatic cancer and glioblastoma (26,30,31). Consistently, the present study

showed that RRM2 knockdown significantly suppressed the proliferation and migration of GC cells while promoting apoptosis. These results suggest that RRM2 plays a crucial role in maintaining the malignant phenotype of GC cells and acts as a key regulator of tumor cell fate during GC progression.

In several cancer types, including breast, lung, cervical, and prostate cancers, higher RRM2 expression is typically associated with shorter OS and progression-free survival, indicating its potential role as a negative prognostic indicator (32-34). However, in the present study, integrated analysis of three independent GC datasets (GSE66229, GSE84433, and TCGA-STAD) revealed a contrasting trend: Patients with GC with higher RRM2 expression exhibited improved survival outcomes. This trend was consistent across all three datasets. Moreover, it was found that RRM2 expression was lower in patients with advanced GC than in those with early-stage GC. These results contradicted the findings of *in vitro* experiments; however, subsequent immune infiltration analysis provided a potential explanation. Immune infiltration analysis revealed that patients with GC with higher RRM2 expression exhibited a more active immune microenvironment, characterized by increased abundances of activated CD4 memory T cells, M0 and M1 macrophages, and resting NK cells and upregulated expression of immune checkpoint genes such as LAG3, PDCD1, and CTLA4. TIMER database prediction showed that patients with high RRM2 expression expressed higher levels of $CD8^+$ T cells, $CD8^+$ naive T cells, CTL and cytotoxic cells. Additionally, GC cells with low RRM2 expression exhibited high TIDE scores, suggesting a reduced likelihood of patient response to immune checkpoint inhibitor therapy. These findings suggest that tumors with high RRM2 expression exhibit greater immunogenicity and can be more readily recognized and targeted by the host immune system. Consistently, previous studies have reported that patients with high RRM2 expression often have high immune scores and are more likely to respond favorably to immunotherapy (19,35,36). Multi-cancer pan-analysis demonstrated that high expression of RRM2 was positively correlated with immune checkpoint genes (including PD-1, PD-L1, CTLA4), tumor mutational burden, and T-cell inflammatory signatures, suggesting its potential as a biomarker for a more immunogenic tumor subtype (37). Research has revealed that RRM2 can upregulate PD-L1 expression via the ANXA1/AKT or ERK pathways, thereby influencing immune evasion and sensitivity to immunotherapy. However, contradictory findings in different cancer types indicate that high RRM2 expression is correlated with reduced $CD8^+$T-cell infiltration and poorer prognosis, highlighting its tissue- and context-dependent immunological implications (38). Based on these findings, it is surmised that high RRM2 expression in malignant gastric epithelial cells promotes tumor cell proliferation while enhancing antitumor immune responses, consequently contributing to improved survival outcomes in patients with GC. This paradoxical role highlights the potential of RRM2 not only as a driver of tumorigenesis but also as a biomarker for predicting immunotherapy response, offering valuable insights for the development of personalized therapeutic strategies for GC.

RRM2 is a crucial rate-limiting enzyme subunit in DNA synthesis and repair (39). Its downregulation has been shown to significantly suppress the proliferative and invasive abilities of GC cell lines such as MKN-1, MKN-7, and SNU-719 (40). Moreover, it was also revealed that high RRM2 expression is closely associated with advanced TNM stages in patients with GC. RRM2 expression has been shown to be markedly upregulated during the S phase of the cell cycle to meet the increased demand for dNTPs during DNA replication (41,42). In the present study, RRM2 knockdown led to the accumulation of DNA DSBs in GC cells, as evidenced by elevated γH2AX expression and pronounced comet tails. These changes were accompanied by a significant reduction in the expression of RAD51, a key component in the HR repair pathway. Conversely, the expression levels of PARP-1, which is involved in SSB, and XRCC1, which is involved in BER repair, remained unchanged. These findings suggest that RRM2 is involved in maintaining genomic stability in GC cells. The observed downregulation of RAD51 and accumulation of γH2AX are consistent with impaired HR repair; however, direct functional assays are warranted to confirm HR deficiency. Although the unchanged PARP-1 and XRCC1 expression levels suggest that BER and SSB repair pathways were not markedly affected by RRM2 knockdown, potential defects cannot be excluded in other repair pathways, such as non-homologous end joining, mismatch repair, and replication fork stabilization. Similar associations between RRM2 expression and DNA repair fidelity have been reported in atypical teratoid rhabdoid tumors. After treatment with the inhibitor of RRM2, the DNA repair signaling signatures were downregulated in atypical teratoid rhabdoid tumor cells, and DNA breaks were induced in the cells. Notably, the HR repair pathway experienced a more pronounced suppression (43). Based on these observations, it was surmised that patients with GC with high RRM2 expression exhibit more efficient DNA repair, which can contribute to improved genomic stability and partially explain the superior survival outcomes observed in these patients.

Compared with previous research (41), the present study redefined the driver population of GC by focusing on malignant epithelial cells, thereby establishing a biologically grounded framework for understanding tumor progression. Through the integration of single-cell transcriptomic data and large clinical cohorts (TCGA/GEO), it was revealed that although RRM2 expression is elevated in GC, its high expression unexpectedly predicts favorable prognosis. Functional assays, including alkaline comet and γH2AX staining, further demonstrated that RRM2 modulates DNA damage accumulation and HR repair, and its expression is associated with an active immune microenvironment. These findings collectively provide novel perspectives that differ fundamentally from prior research (44). However, the present study has several limitations. Multivariate Cox regression could not be performed because only limited clinical variables (sex, age, and TNM stage) were available, while key factors such as differentiation grade, treatment, and molecular subtype were missing. This limitation may reduce the ability of the model to account for confounding effects. Although the present study indicates that RRM2 is transcriptionally upregulated in GC, protein-level validation was not performed owing to the limited availability of matched proteomic data. Future studies incorporating proteomic analysis are warranted to confirm the regulatory functions of RRM2 in GC. Moreover, concurrent mRNA-level validation of RAD51 downregulation should be

prioritized in future studies. This would not only corroborate the observed protein-level changes but also clarify whether RAD51 suppression occurs through transcriptional repression or post-translational mechanisms such as ubiquitin-mediated degradation. Elevated γH2AX signals DNA damage accumulation, but cannot differentiate its source, such as replication stress, nucleotide depletion, or oxidative stress. Therefore, additional studies are needed to pinpoint the exact cause after RRM2 knockdown. The lack of *in vivo* models limits the ability to fully validate the role of RRM2 in tumor progression within the complex tumor immune microenvironment of GC. Moreover, the mechanistic relationship between RRM2 expression and improved prognosis remains speculative, as direct functional evidence, particularly concerning immune activation and immunotherapy response, remains lacking. In addition, the findings require validation in larger, multi-center clinical cohorts to ensure their generalizability. To address these gaps, future studies should focus on generating RRM2 gene-edited GC mouse models to investigate the effects of RRM2 on tumor growth, metastasis, and immune modulation *in vivo*. Incorporating functional HR experiments, such as DR-GFP assay or sensitivity analysis of PARP inhibitors, should be the focus of follow-up studies. The DR-GFP reporter assay directly measures HR repair efficiency post-DNA double-strand break induction (45), assessing whether RRM2 knockdown compromises HR-mediated DNA repair. HR-deficient cells accumulate unrepaired DNA damage, becoming hypersensitive to PARP inhibition (46). The present study evaluated whether RRM2 depletion enhances cellular sensitivity to PARP inhibitors. Prospective clinical studies with larger sample sizes are planeed to elucidate the clinical relevance of RRM2 in personalized treatment strategies for GC. In conclusion, through integrated multi-omic analysis, the present study elucidated the expression profile and functional role of RRM2 in GC, highlighting its potential as a key driver of malignant progression and a promising target for immunotherapy in GC. Future studies incorporating animal models and clinical specimens are warranted to promote the clinical application of RRM2 in the early detection and precise treatment of GC.

Acknowledgements

Not applicable.

Funding

No funding was received.

Availability of data and materials

The data generated in the present study may be requested from the corresponding author.

Authors' contributions

YH, DZ and MW conceived the present study. XC and MW performed the methodology, formal analysis, investigation, and visualization. XC wrote and prepared the original draft. YH and TM wrote reviewed and edited the manuscript. TM performed the data analysis and interpretation. XC and TM confirm the authenticity of all the raw data. All authors read and approved the final manuscript.

Ethics approval and consent to participate

Not applicable.

Patient consent for publication

Not applicable.

Competing interests

The authors declare that they have no competing interests.

Use of artificial intelligence tools

During the preparation of this work, artificial intelligence tools were used to improve the readability and language of the manuscript or to generate images, and subsequently, the authors revised and edited the content produced by the artificial intelligence tools as necessary, taking full responsibility for the ultimate content of the present manuscript.

References

1. Sundar R, Nakayama I, Markar SR, Shitara K, van Laarhoven HWM, Janjigian YY and Smyth EC: Gastric cancer. Lancet 405: 2087-2102, 2025.
2. Yang X, Zhang J, Ma J, Huang J, Wang Y, Wang P, Wang F and Tang X: GPER governs the immune infiltration of gastric cancer and activates the NF-κB/ROS/Apoptosis pathway in gastric mucosal epithelium. Int Immunopharmacol 122: 110641, 2023.
3. Bray F, Laversanne M, Sung H, Ferlay J, Siegel RL, Soerjomataram I and Jemal A: Global cancer statistics 2022: GLOBOCAN estimates of incidence and mortality worldwide for 36 cancers in 185 countries. CA Cancer J Clin 74: 229-263, 2024.
4. Lordick F, Carneiro F, Cascinu S, Fleitas T, Haustermans K, Piessen G, Vogel A and Smyth EC; ESMO Guidelines Committee. Electronic address: clinicalguidelines@esmo.org: Gastric cancer: ESMO clinical practice guideline for diagnosis, treatment and follow-up. Ann Oncol 33: 1005-1020, 2022.
5. Zhao L, Huang H, Zhang C, Luan X, Niu P, Zhu Y, Xiong Y, Wang W, Han X, Huang D, *et al*: Temporospatial variation in environmental risk factors and related gastric cancer incidence: A registry-based study in an area with the largest gastric cancer burden in China. J Glob Health 15: 04083, 2025.
6. Zhou L, Han B, Yuan Y, Dong Z, Shi Y and Zheng R: The global burden of stomach cancer and its risk factors from 1990 to 2021: Findings from the global burden of disease study 2021. BMC Public Health 25: 2678, 2025.
7. Petrillo A and Smyth EC: Biomarkers for precision treatment in gastric cancer. Visc Med 36: 364-372, 2020.
8. Gao YX, Guo XJ, Lin B, Huang XB, Tu RH, Lin M, Cao LL, Chen QY, Wang JB, Xie JW, *et al*: Targeting LHPP in neoadjuvant chemotherapy resistance of gastric cancer: Insights from single-cell and multi-omics data on tumor immune microenvironment and stemness characteristics. Cell Death Dis 16: 306, 2025.
9. Zhou J, Li J, Chen J, Lan X, Ai Y, Liu P, Peng J, Pan X, Zhang Y, Zhang H, *et al*: Decoding inflammatory mediators in the Correa's cascade: From chronic gastritis to carcinogenesis and targeted therapies. Int Immunopharmacol 162: 115191, 2025.
10. Shi Y, Jia E, Wu X and Wang F: Upregulation of MFAP5 enhances COL1A1 expression, promoting epithelial-mesenchymal transition in gastric cancer cells. Discov Med 36: 2079-2087, 2024.
11. Coorens THH, Collord G, Jung H, Wang Y, Moore L, Hooks Y, Mahbubani K, Law SYK, Yan HHN, Yuen ST, *et al*: The somatic mutation landscape of normal gastric epithelium. Nature 640: 418-426, 2025.

12. Liu B, Liu H, Ren F, Liu H, Bukhari I, Fu Y, Wu W, Zhao M, Zhu S, Mo H, *et al*: cGAS regulates the DNA damage response to maintain proliferative signaling in gastric cancer cells. Oncol Res 29: 87-103, 2021.
13. Hu H, Yang H, Fan S, Jia X, Zhao Y and Li H: LncRNA HOTAIR promotes DNA damage repair and radioresistance by targeting ATR in colorectal cancer. Oncol Res 32: 1335-1346, 2024.
14. Kaiser L, Ondrus M, Slavetinska LP, Raindlova V and Hocek M: Polymerase synthesis of hypermodified DNA displaying a combination of thiol, hydroxyl, carboxylate, and imidazole functional groups in the major groove. Chemistry 31: e202501034, 2025.
15. Garzon J, Rodriguez R, Kong Z, Chabes A, Rodriguez-Acebes S, Mendez J, Moreno S and García-Higuera I: Shortage of dNTPs underlies altered replication dynamics and DNA breakage in the absence of the APC/C cofactor Cdh1. Oncogene 36: 5808-5818, 2017.
16. Long MJC, Van Hall-Beauvais A and Aye Y: The more the merrier: How homo-oligomerization alters the interactome and function of ribonucleotide reductase. Curr Opin Chem Biol 54: 10-18, 2020.
17. Guo L, Zhao Y, Bai X, Wang X, Tuoheti K, Cao Y, Zuo Y, Zhang X and Liu T: RRM2 is a putative biomarker and promotes bladder cancer progression via PI3K/AKT/mTOR pathway. J Cell Physiol 240: e31501, 2025.
18. Liu K, Wang L, Lou Z, Guo L, Xu Y, Qi H, Fang Z, Mei L, Chen X, Zhang X, *et al*: E2F8 exerts cancer-promoting effects by transcriptionally activating RRM2 and E2F8 knockdown synergizes with WEE1 inhibition in suppressing lung adenocarcinoma. Biochem Pharmacol 218: 115854, 2023.
19. Mao G, Li L, Shan C, Liang B, Ma L and Zhang S: High expression of RRM2 mediated by non-coding RNAs correlates with poor prognosis and tumor immune infiltration of hepatocellular carcinoma. Front Med (Lausanne) 9: 833301, 2022.
20. Shi SC, Zhang Y and Wang T: High RRM2 expression has poor prognosis in specific types of breast cancer. PLoS One 17: e0265195, 2022.
21. Abdel-Rahman MA, Mahfouz M and Habashy HO: RRM2 expression in different molecular subtypes of breast cancer and its prognostic significance. Diagn Pathol 17: 1, 2022.
22. Oh SC, Sohn BH, Cheong JH, Kim SB, Lee JE, Park KC, Lee SH, Park JL, Park YY, Lee HS, *et al*: Clinical and genomic landscape of gastric cancer with a mesenchymal phenotype. Nat Commun 9: 1777, 2018.
23. Cheong JH, Yang HK, Kim H, Kim WH, Kim YW, Kook MC, Park YK, Kim HH, Lee HS, Lee KH, *et al*: Predictive test for chemotherapy response in resectable gastric cancer: A multicohort, retrospective analysis. Lancet Oncol 19: 629-638, 2018.
24. Jiang H, Yu D, Yang P, Guo R, Kong M, Gao Y, Yu X, Lu X and Fan X: Revealing the transcriptional heterogeneity of organ-specific metastasis in human gastric cancer using single-cell RNA Sequencing. Clin Transl Med 12: e730, 2022.
25. Liang CC, Park AY and Guan JL: In vitro scratch assay: A convenient and inexpensive method for analysis of cell migration in vitro. Nat Protoc 2: 329-333, 2007.
26. Zhan Y, Jiang L, Jin X, Ying S, Wu Z, Wang L, Yu W, Tong J, Zhang L, Lou Y and Qiu Y: Inhibiting RRM2 to enhance the anticancer activity of chemotherapy. Biomed Pharmacother 133: 110996, 2021.
27. Zuo Z, Zhou Z, Chang Y, Liu Y, Shen Y, Li Q and Zhang L: Ribonucleotide reductase M2 (RRM2): Regulation, function and targeting strategy in human cancer. Genes Dis 11: 218-233, 2024.
28. Wang XJ, Huo YX, Yang PJ, Gao J and Hu WD: Significance of ribonucleoside-diphosphate reductase subunit M2 in lung adenocarcinoma. Curr Gene Ther 25: 136-156, 2025.
29. Han P, Chen RH, Wang F, Zeng JY, Yu ST, Xu LH, Cai Q, Liang FY, Xia TL, Lin ZR, *et al*: Novel chimeric transcript RRM2-c2orf48 promotes metastasis in nasopharyngeal carcinoma. Cell Death Dis 8: e3047, 2017.
30. Liu Q, Song C, Li J, Liu M, Fu L, Jiang J, Zeng Z and Zhu H: E2F2 enhances the chemoresistance of pancreatic cancer to gemcitabine by regulating the cell cycle and upregulating the expression of RRM2. Med Oncol 39: 124, 2022.
31. Perrault EN, Shireman JM, Ali ES, Lin P, Preddy I, Park C, Budhiraja S, Baisiwala S, Dixit K, James CD, *et al*: Ribonucleotide reductase regulatory subunit M2 drives glioblastoma TMZ resistance through modulation of dNTP production. Sci Adv 9: eade7236, 2023.
32. Ma C, Luo H, Cao J, Gao C, Fa X and Wang G: Independent prognostic implications of RRM2 in lung adenocarcinoma. J Cancer 11: 7009-7022, 2020.
33. Wang J, Yi Y, Chen Y, Xiong Y and Zhang W: Potential mechanism of RRM2 for promoting cervical cancer based on weighted gene co-expression network analysis. Int J Med Sci 17: 2362-2372, 2020.
34. Cheng B, Li L, Wu Y, Luo T, Tang C, Wang Q, Zhou Q, Wu J, Lai Y, Zhu D, *et al*: The key cellular senescence related molecule RRM2 regulates prostate cancer progression and resistance to docetaxel treatment. Cell Biosci 13: 211, 2023.
35. Zhou Z, Song Q, Yang Y, Wang L and Wu Z: Comprehensive landscape of RRM2 with immune infiltration in pan-cancer. Cancers (Basel) 14: 2938, 2022.
36. Lee SK, Hwang Y, Han JH, Haam S, Lee HW and Koh YW: Characteristics of the immune microenvironment associated with RRM2 expression and its application to PD-L1/PD-1 inhibitors in lung adenocarcinoma. Am J Cancer Res 13: 5443-5454, 2023.
37. Wu L, Yin L, Ma L, Yang J, Yang F, Sun B and Nianzeng X: Comprehensive bioinformatics analysis of ribonucleoside diphosphate reductase subunit M2(RRM2) gene correlates with prognosis and tumor immunotherapy in pan-cancer. Aging (Albany NY) 14: 7890-7905, 2022.
38. Wang Y, Chen R, Zhang J and Zeng P: A comprehensive analysis of ribonucleotide reductase subunit M2 for carcinogenesis in pan-cancer. PLoS One 19: e0299949, 2024.
39. Tan J, Wang W, Liu X, Xu J, Che Y, Liu Y, Hu J, Hu L, Li J and Zhou Q: C11orf54 promotes DNA repair via blocking CMA-mediated degradation of HIF1A. Commun Biol 6: 606, 2023.
40. Morikawa T, Hino R, Uozaki H, Maeda D, Ushiku T, Shinozaki A, Sakatani T and Fukayama M: Expression of ribonucleotide reductase M2 subunit in gastric cancer and effects of RRM2 inhibition in vitro. Hum Pathol 41: 1742-1748, 2010.
41. Ping S, Jia X and Tian Y: Integration of scRNA-seq and ST-seq identifies hyperproliferative RRM2+ cells features and therapeutic targets in gastric cancer. J Transl Med 23: 795, 2025.
42. Sun X, Duan K, Shen X, Dong C, Zhou Y, Chen T, Li W, Li P, Wang P, Li D and Zhou J: Construction and validation of a nomogram model for predicting peritoneal metastasis in gastric cancer based on ferroptosis-relate genes and clinicopathological features. J Gastrointest Oncol 16: 264-280, 2025.
43. Giang LH, Wu KS, Lee WC, Chu SS, Do AD, Huang MH, Lin YL, Hsieh CL, Sung SY, Yen Y, *et al*: RRM2 inhibition alters cell cycle through ATM/Rb/E2F1 pathway in atypical teratoid rhabdoid tumor. Neoplasia 58: 101075, 2024.
44. Luo XJ, Lu YX, Wang Y, Huang R, Liu J, Jin Y, Liu ZK, Liu ZX, Huang QT, Pu HY, *et al*: M6A-modified lncRNA FAM83H-AS1 promotes colorectal cancer progression through PTBP1. Cancer Lett 598: 217085, 2024.
45. Vriend LE, Jasin M and Krawczyk PM: Assaying break and nick-induced homologous recombination in mammalian cells using the DR-GFP reporter and Cas9 nucleases. Methods Enzymol 546: 175-191, 2014.
46. Zhang N, Tian YN, Zhou LN, Li MZ, Chen HD, Song SS, Huan XJ, Bao XB, Zhang A, Miao ZH and He JX: Glycogen synthase kinase 3beta inhibition synergizes with PARP inhibitors through the induction of homologous recombination deficiency in colorectal cancer. Cell Death Dis 12: 183, 2021.